Powder Technology 487 (2027) 123424

Contents lists available at ScienceDirect

Powder Technology

journal homepage: www.journals.elsevier.com/powder-technology

A hybrid analytical model for the packing of frictional spheroidal particles

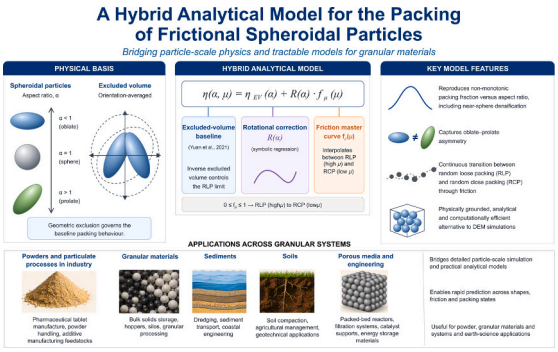
David A. Robinson [a,*], Sarem Norouzi [b], Amy Thomas [a], Lis Wollesen de Jonge [b], Shmulik P. Friedman [c]

[a] UK Centre for Ecology & Hydrology, Deiniol Road, Bangor LL57 2UW, UK
[b] Department of Agroecology, Aarhus University, Tjele, Denmark
[c] The Institute of Soil, Water and Environmental Sciences, Agricultural Research Organization, The Volcani Center, Rishon LeZion 7505101, Israel

HIGHLIGHTS

- Develops a hybrid analytical model for frictional spheroidal particle packings.
- Extends excluded-volume theory using a symbolic-regression-derived correction.
- Reproduces near-sphere densification and oblate–prolate packing asymmetry.
- Bridges random loose and random close packing through friction-dependent interpolation.
- Provides a computationally efficient alternative to DEM-based packing predictions.

GRAPHICAL ABSTRACT



ARTICLE INFO

Keywords:
Bulk density
Particle shape
Sediment
Soil
Porosity

ABSTRACT

The packing of nonspherical particles remains a fundamental challenge in granular physics and powder technology because particle shape and interparticle friction jointly control packing density, porosity and microstructure. Existing excluded-volume models successfully describe many aspects of frictional particle packings but do not fully reproduce the characteristic densification peak observed for spheroids near unit aspect ratio. In this study, we develop a friction-dependent analytical model for the packing fraction of isotropically packed spheroidal particles by extending a literature based excluded-volume framework. The model combines an excluded-volume baseline with an additional shape-dependent rotational correction identified using symbolic regression, while a friction-dependent master curve is used to interpolate continuously between random loose and random close packing limits. The resulting formulation spans aspect ratios from highly oblate to highly prolate spheroids and reproduces the characteristic non-monotonic variation of packing fraction with particle shape, including near-sphere densification, the decline in packing efficiency at extreme aspect ratios, and the observed asymmetry between oblate and prolate packings. Model predictions show good agreement with published experimental and simulation datasets across a wide range of aspect ratios and friction states. The proposed framework provides a compact and physically interpretable alternative to computationally intensive simulations for practical application and testing.

* Corresponding author.
E-mail address: David.Robinson@ceh.ac.uk (D.A. Robinson).

https://doi.org/10.1016/j.powtec.2026.123424
Received 9 July 2026; Received in revised form 12 October 2026; Accepted 26 October 2026
Available online 27 October 2026
0032-5910/© 2026 The Authors. Published by Elsevier B.V. This is an open access article under the CC BY license (http://creativecommons.org/licenses/by/4.0/).

1. Introduction

The packing of nonspherical particles remains a fundamental problem in powder technology because particle shape and interparticle friction strongly influence bulk density, porosity, flowability, permeability, and mechanical stability [1]. Unlike spheres, anisotropic particles possess additional rotational degrees of freedom, orientation-dependent excluded volumes, and shape-specific contact constraints that produce more complex packing behaviour [1,2]. Experiments and simulations consistently show that spheroids exhibit a non-monotonic relationship between aspect ratio and packing fraction: packing density increases as particles deviate slightly from spherical geometry, reaches a maximum at moderate asphericity, and then decreases for highly elongated or flattened particles [3–6]. This characteristic behaviour reflects a competition between orientational freedom, which promotes denser local arrangements, and increasing excluded volume, which progressively reduces packing efficiency at extreme aspect ratios.

Numerical approaches such as discrete element modelling, molecular dynamics, and mechanical contraction algorithms have significantly advanced understanding of spheroidal packings and generated extensive benchmark datasets [4,6–8]. However, these methods are computationally expensive, preparation-protocol dependent, and do not yield compact analytical relationships suitable for incorporation into continuum-scale powder, granular, or porous-media models [9]. Consequently, considerable interest remains in analytical formulations that retain a clear physical basis while reproducing the key features observed in experiments and simulations. Excluded-volume theory has been particularly successful in this regard, linking packing fraction directly to particle geometry through the orientation-averaged excluded volume [5,10–12]. Recent work by Yuan et al. [8] developed a universal friction-dependent framework for jammed packings that successfully describes random loose packing across a wide range of particle shapes.

Despite this progress, existing analytical excluded-volume models do not fully reproduce the pronounced densification peak observed for spheroids near unit aspect ratio. Simulations and experiments consistently show that slightly oblate and prolate spheroids can pack more densely than spheres, achieving packing fractions of approximately 0.70–0.71 compared with about 0.64 for random close-packed spheres [3,4,6]. Moreover, numerical studies have shown that prolate spheroids can achieve marginally higher maximum packing fractions than oblate spheroids, for a similar departure from spherical geometry [3,4,8]. This near-spherical enhancement is thought to arise from orientational correlations and rotational freedom that become increasingly important at low friction but are not explicitly represented in current excluded-volume formulations. Existing compact models also struggle to reproduce the subtle asymmetry between oblate and prolate packing maxima within a single friction-dependent framework.

In this study, we develop a friction-dependent analytical model for the packing fraction of isotropically packed spheroids that extends the excluded-volume framework of Yuan et al. [8] through the addition of a shape-dependent rotational correction term. The correction is identified using symbolic regression applied to residuals between benchmark packing data and the excluded-volume baseline model, yielding a compact and interpretable closed-form expression. By scaling this correction with the friction master curve of Yuan et al., [8] the model continuously transitions from the frictionless random close packing limit to the high-friction random loose packing regime. The resulting formulation reproduces the near-sphere densification peak, captures the observed minor oblate-prolate asymmetry, and provides a simple analytical framework for predicting the packing behaviour of frictional spheroidal particles across a wide range of aspect ratios without requiring computationally intensive particle-scale simulations.

2. Methods

2.1. Spheroid geometry

Spheroidal particles are ellipsoids defined by two equal equatorial semi-axes a aligned with the x–y plane and a polar semi-axis c aligned with the z-direction (Fig. 1). When a = c, the particle reduces to a sphere with unit aspect ratio ($\alpha = 1$). Oblate spheroids ($c < a$, $\alpha < 1$) adopt disk-like morphologies, whereas prolate spheroids ($c > a$, $\alpha > 1$) are elongated or needle-like, as illustrated schematically in Fig. 1. These geometric distinctions control excluded volume, coordination number, and rotational accessibility, thereby governing packing efficiency, porosity, and mechanical stability in granular assemblies. The influence of particle shape on the densest achievable packing is commonly interpreted through the number of accessible degrees of freedom (DOF). While rigid-body motion is formally described by six degrees of freedom (three translational, x,y,z and three rotational, θ_x,θ_y,θ_z (Fig. 1)), packing behaviour depends only on those motions that alter interparticle contacts. Following the constraint-counting framework of Donev, Torquato, Stillinger and Connelly [13], a sphere has three effective degrees of freedom because all rotations are symmetry-equivalent and leave the contact geometry unchanged. Oblate and prolate spheroids possess five effective degrees of freedom, since rotation about the symmetry axis (θ_z; Fig. 1) leaves the configuration invariant, whereas rotations about the remaining axes (θ_x, θ_y) alter contact geometry. In contrast, a triaxial ellipsoid lacks rotational symmetry and therefore retains all six effective degrees of freedom, with every translational and rotational motion producing a distinct configuration. This symmetry-reduced hierarchy of effective degrees of freedom directly influences jamming constraints and enables non-spherical particles, particularly spheroids, to access a broader configurational space of mechanically stable packings and thus achieve higher packing densities than spheres.

2.2. Model development using excluded volume

From a conceptual viewpoint, particle packing is often considered as starting with the dilute limit through the ideal gas equation and statistical mechanics.

$$PV/NkT = Z = 1 \tag{1}$$

Where, P, is the pressure, V, is the volume, N, is the number of particles, k_B is Boltzmann's constant and T is temperature, Z is the structural compressibility factor [14]. In the absence of interactions between particles, when they are far from each other (i.e., an ideal gas), the compressibility factor has Z = 1 as in Eq. (1). However, as a granular material becomes denser, this no longer holds and under compression a gas can be considered to undergo a transition to a dense gas, a liquid, and ultimately to a granular or crystalline solid material. The correlation effects, which refer to the influence that the positions or orientations of particles have on each other beyond what would be expected if they were distributed independently, are described by Z becoming a virial expansion. The series is expressed in terms of the number density $\rho = N/V$, and the expansion is written in powers of ρ:

$$Z = 1 + B_2\rho + B_3\rho^2 + \cdots = 1 + B_2\frac{N}{V} + B_3\left(\frac{N}{V}\right)^2 + \cdots \tag{2}$$

The second virial coefficient B_2 accounts for pairwise interactions between particles Eq. (2). For hard particles (i.e., particles that interact only via excluded volume and cannot penetrate each other), B_2 is directly related to the excluded volume V_{ex} between two particles (for identical hard bodies, the second virial coefficient is $B_2 = ½\ V_{ex}$; in packing theory V_{ex} is typically, rather than a half is used directly). Third virial coefficient B_3, and higher orders, effectively quantify the additional excluded volume due to three particles or more coming into close contact in ways not accounted for by just adding up pairwise exclusions.

In the context of particle packings and jamming, the simplest excluded-volume descriptions operate at the second-virial level: they retain only pairwise steric interactions and neglect three-body and higher-order correlations. This is sometimes referred to as a mean-field treatment because the detailed spatial correlations of neighbours are replaced by an orientation-averaged excluded volume. In this sense, the model assumes that neighbours are arranged randomly (uncorrelated), and mechanical stability is controlled primarily by the average two-particle exclusion volume. Many theoretical models of random loose packing (RLP) use this approach. For example, the pioneering work of Onsager [11] on liquid crystal theory treated orientationally averaged excluded volume (a two-body property) as the key to predicting phases. Similarly, Philipse [12] applied a mean-field excluded-volume argument to spherocylinders Eq. (3), relating the average contact number $\langle C\rangle$ and number density ρ through the excluded volume of a particle pair. This yields an approximate packing fraction formula under the assumption of uncorrelated (random) contacts [6,12,15,16]:

$$\eta = \langle C\rangle \cdot \frac{v_p}{\langle V_{\mathrm{ex}}\rangle} \tag{3}$$

where $\langle C\rangle$ is shape-independent and determined by the marginal stability condition (related to the mean contact number at the jamming threshold), and the exclusion fraction ($v_p/\langle V_{ex}\rangle$) is the particle volume over, $\langle V_{ex}\rangle$ which is the orientation-averaged excluded volume. For rods/sphero-cylinders, Philipse [12] reported a value of 10.8 ± 0.4 for $\langle C\rangle$, while Williams and Philipse [5] found a value of 10.2, and Wouterse, Luding and Philipse [16] provided an experimental measurement of 9.8, which aligns with the modelling results of Donev [3]. This expression is essentially an ideal packing law assuming uncorrelated contacts – it mirrors a second-virial (pair-exclusion) approximation where each contact is treated as independent (no triplet or higher-order clustering effects). Under such assumptions, packing fraction is predicted to decrease in direct proportion to $1/\langle V_{\mathrm{ex}}\rangle$. Notably, this excluded-volume mean-field model predicts that more aspherical particles (which have larger excluded volume $\langle V_{\mathrm{ex}}\rangle$) will always pack less densely, all else being equal. This trend is observed in experiments and simulations for very loose, random packings where particles are free to arrange without significant ordering.

However, as packings densify or become more mechanically constrained, the "uncorrelated contact" assumption breaks down and higher-order correlations (many-body interactions) come into play. In such regimes – for example, approaching random close packing (RCP = 0.64) e.g. when friction is low – particles can form local structures that are not entirely random, they may have slight orientational alignment or clustering [7,17]. In terms of the virial expansion, these structural correlations mean that third and higher virial coefficients (like B_3) contribute significantly to the system's behaviour. Indeed, it has been noted that truly ideal (second-virial dominated) behaviour is absent in maximally dense random sphere packings; monodisperse spheres at RCP exhibit substantial many-body correlations (e.g. local crystalline-like arrangements), so their packing cannot be predicted by a simple two-body excluded-volume model alone. In other words, jammed sphere packings are "non-ideal" because each particle's environment is influenced by cooperative interactions among multiple neighbours, not just isolated pairs.

Yuan, Jiao, Wang and Li [8] found that in the limit of infinite friction, jammed packings of various nonspherical particles reach the Random Loose Packing (RLP) state, which is characterized by minimal coordination number (close to the isostatic minimum for frictional particles) and very weak structural correlations. In this RLP regime, the packing fraction for all particle shapes was observed to be a simple monotonic function of the orientation-averaged excluded volume – essentially validating a mean-field excluded-volume (second-virial) model for the loosest stable packings. In other words, the Yuan, Jiao, Wang and Li [8] RLP data support the idea that jamming at high friction is governed primarily by pairwise excluded-volume constraints (each particle just "sees" the total excluded volume of its neighbours, without significant higher-order ordering). This is why Yuan, Jiao, Wang and Li [8] report a "simple scaling" of η with $\langle V_{\mathrm{ex}}\rangle$ in the RLP limit – it's essentially the same scaling one would get from the idealized packing law described previously. Their work confirms earlier geometric packing studies by [5,12] who likewise showed that if you plot random packing density as a function of a shape parameter related to excluded volume, data for many different shapes collapse onto a universal curve, indicating the dominance of excluded-volume (second-virial-like) effects in loose random packing.

When friction is finite or zero, however, packings become denser and exhibit more pronounced short-range order (e.g., slight alignment of neighbour particles, layering, etc. Delaney, Hilton and Cleary [7]). Yuan, Jiao, Wang and Li [8] describe packings with finite friction as continuously departing from the RLP reference state via increasing structural correlations ("a perturbative approach based on RLP" as they phrase it). In practical terms, as friction decreases, particles can rearrange into more efficient, but also more correlated, configurations. This is where higher-order virial terms like B_3 become relevant. The model of Yuan, Jiao, Wang and Li [8] for RLP adds a second-order excluded-volume term, which effectively encodes three-body (and higher) interactions analogous to the third virial coefficient B_3. In their 2021 study, Yuan and co-workers found that the packing fraction η of jammed frictional particles could be fit with an empirical two-term equation involving the dimensionless excluded volume Eq. (4). In simplified form, one can write this relationship as:

$$\eta = \mathrm{C}_1\left(\frac{v_p}{V_{ex}}\right) - \mathrm{C}_2\left(\frac{v_p}{V_{ex}}\right)^2 \tag{4}$$

The model, a perturbation expansion, expresses packing fraction η as

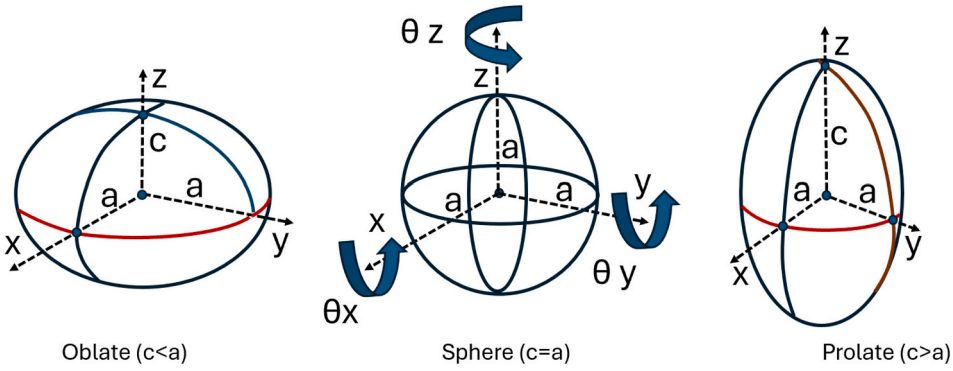


Fig. 1. Schematic comparison of an oblate spheroid, sphere, and prolate spheroid showing geometry, principal axes, and rotational degrees of freedom. Oblate ($c < a$) and prolate ($c > a$) spheroids exhibit axial symmetry about z, such that rotation about the symmetry axis does not alter contact geometry, whereas tilting rotations are distinct. Curved arrows denote rotational modes θ_x, θ_y, and θ_z.

a function of exclusion fraction, ($\nu_p/\langle V_{ex}\rangle$), C_1 is the shape-independent constant determined by the marginal stability condition, while C_2 is an empirical constant that addresses higher-order steric interactions (correlation) among particles. The first term represents the leading mean-field contribution based on pairwise excluded volume (comparable to a second-virial term). This is essentially the "ideal" packing law for completely uncorrelated contacts. This term alone Eq. (3) would imply that the packing fraction of a disordered packing is solely determined by two-particle geometric exclusion, ("second-virial level" approximation), since it considers only binary interactions. However, Yuan, Jiao, Wang and Li [8] observed that for nearly-spherical shapes or conditions with slight ordering, this one-term model is not sufficiently accurate – small systematic deviations appear because real packings are not perfectly uncorrelated. In other words, residual multi-particle correlations (beyond random pair exclusions) affect the packing efficiency. To capture this, Yuan, Jiao, Wang and Li [8] introduced the second term in the equation Eq. (4). This term involves the square of the inverse excluded volume, and is a phenomenological correction for higher-order "steric" interactions. In virial-expansion language, it plays a role analogous to the third (and higher) virial coefficients: it accounts for three-body overlaps and other cooperative packing effects that are not accounted for by the pure two-body (excluded volume) term. Moreover, the second term signals that *jamming is not governed by pure two-body exclusion alone* – especially not for aspherical particles and for conditions slightly above the RLP limit.

The coefficients C_1 and C_2 in Eq. (4) were estimated separately for random loose and random close packing. The orientation-averaged excluded-volume ratio V_{ex}/v_p was calculated for each aspect ratio using the analytical expressions for oblate and prolate spheroids, and the model was fitted using $= v_p/V_{ex}$. The fits were constrained to reproduce packing fractions of 0.55 and 0.64 at the spherical limit, where x = 1/8, for RLP and RCP, respectively. All RLP observations were used, whereas the RCP calibration was restricted to AR > 2.5 to estimate the excluded-volume response outside the near-spherical densification region. Parameter uncertainty was quantified using 5000 non-parametric bootstrap resamples, from which bootstrap standard errors, bias estimates, and percentile-based 95% confidence intervals were calculated.

The constrained fitting procedure results are shown in detail in the supplementary information with produced coefficient values of $C_1 = 7.465$ and $C_2 = 24.522$ for the RLP dataset, and $C_1 = 13.499$ and $C_2 = 67.034$ for the RCP dataset. The coefficients differ slightly for RLP compared to [8] as they were calculated using different model predictions and were anchored at RLP = 0.55 for spheres. The larger coefficients obtained for the RCP calibration reflect the greater packing efficiency of densely packed spheroids, resulting in systematically higher packing fractions across the aspect-ratio range. In both cases, the fitted coefficients satisfy the imposed spherical boundary conditions exactly, reproducing packing fractions of 0.55 and 0.64 at AR = 1 for the

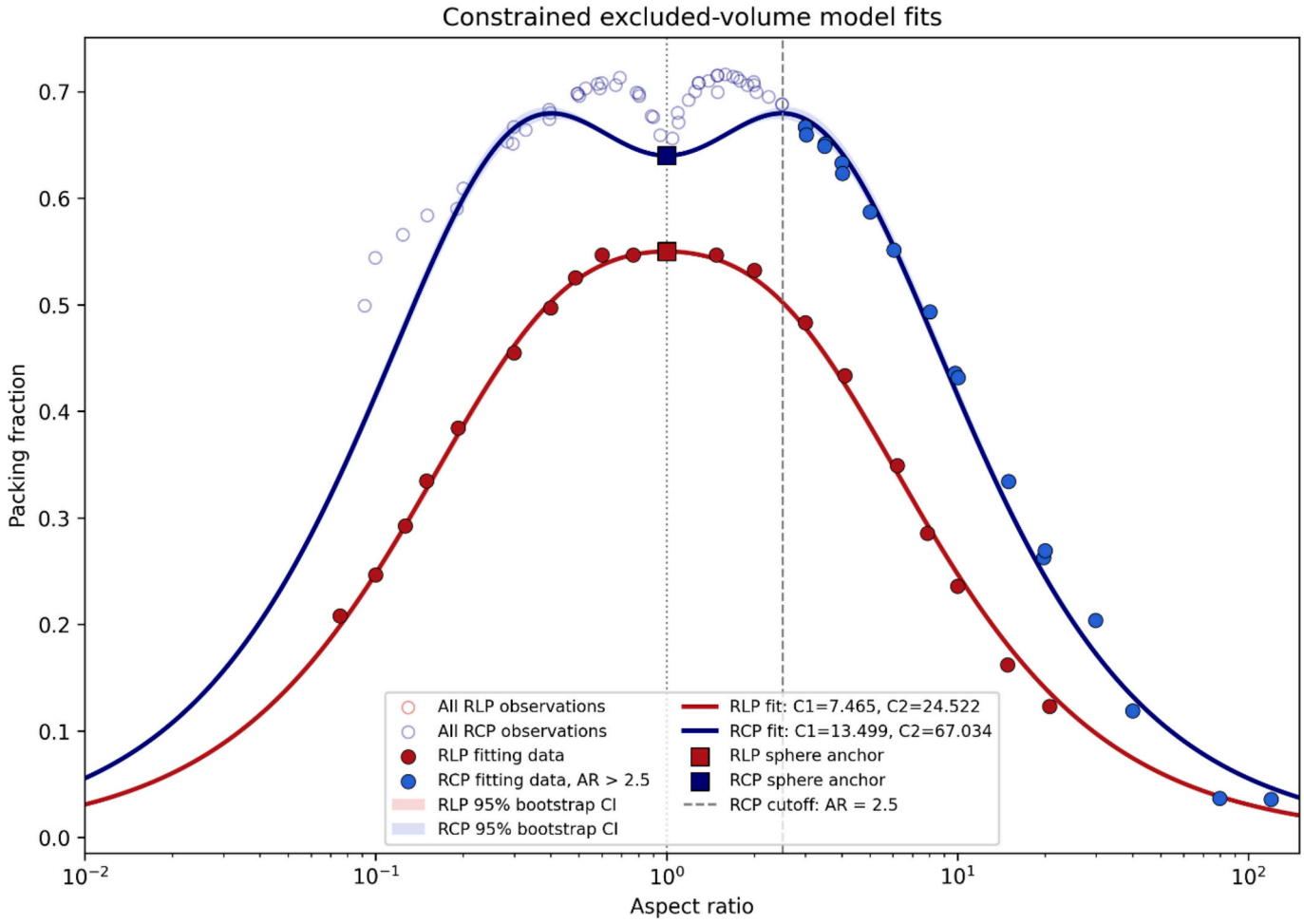


Fig. 2. Packing fraction as a function of particle aspect ratio for the constrained excluded-volume models representing random loose packing (RLP, red) and random close packing (RCP, blue). Symbols show the computational values used for model fitting, while solid lines denote the fitted model predictions constrained to sphere-packing fractions of 0.55 (RLP) and 0.64 (RCP). Shaded regions represent the 95% bootstrap confidence intervals of the fitted curves. Open symbols indicate observations excluded from fitting, and the vertical dashed line marks the aspect-ratio threshold (AR = 2.5) applied in the RCP calibration. (For interpretation of the references to colour in this figure legend, the reader is referred to the web version of this article.)

RLP and RCP states, respectively. Fig. 2 demonstrates that the constrained excluded-volume model captures the broad dependence of packing fraction on particle aspect ratio for both loose and dense packing states. The RLP calibration reproduces the monotonic reduction in packing fraction away from the spherical limit, while the RCP calibration accurately represents the decline in packing fraction observed for highly elongated particles (AR > 2.5). The narrow bootstrap confidence envelopes indicate relatively low parameter uncertainty within the calibration domain, suggesting that the fitted coefficients are robust to resampling of the available observations. Consistent with the underlying excluded-volume framework, the model reproduces the large-scale shape dependence of spheroidal packing while intentionally excluding the near-spherical densification peak from the RCP calibration, which is addressed separately through the symbolic-regression correction presented later on.

The findings of Yuan, Jiao, Wang and Li [8] thereby bridge the gap between a simple mean-field like theory and the more complex reality of jammed matter: in the frictional RLP limit, the packing behaves almost like a second-virial (excluded-volume) 'ideal gas' of particles, whereas departures from this ideal — through reduced friction or shape-induced correlations — introduce higher-order geometrical structure, which the second term captures surprisingly well when the model is compared with simulated data (Fig. 2). This interpretation is consistent with earlier geometric packing studies and the concept of isochoric ideality by Kyrylyuk, van de Haar, Rossi, Wouterse and Philipse [18]: suggesting that jamming is largely controlled by pairwise excluded-volume geometry at RLP, with three-body (and higher) effects becoming important as packings become denser or particles more aspherical. Robinson, Friedman, Thomas, Hirmas, Sullivan and Nemes [9] found this was also reasonable for MRJ packings. However, it was clear that it failed to capture the behaviour at low aspect ratios close to spheres as it doesn't account for rotational degrees of freedom, which are essential for the spheroid RCP peak (Fig. 2). Robinson, Friedman, Thomas, Hirmas, Sullivan and Nemes [9] suggested this could be addressed by adding a third empirical term to the model, that essentially accounts for rotational alignment around RCP. The proposed approach offered a conceivable path to extend the perturbation expansion of [8] into a functioning hybrid packing model that operates across the range of packing from RLP to RCP, but the approach would benefit from some refinement and accounting for changing friction, not considered in Robinson, Friedman, Thomas, Hirmas, Sullivan and Nemes [9].

2.3. Symbolic regression in model development

The mathematical form that a rotational alignment correction should take is unknown. Robinson, Friedman, Thomas, Hirmas, Sullivan and Nemes [9] used an empirical Jacquelin Generalised Logistic With Offset [19] as a function of aspect ratio to model the RCP limit. However, in this work, we turn to the use of symbolic regression to try and find a more compact, elegant term that can be added to the model to account for rotational alignment as a function of aspect ratio through excluded volume. Physically, this term represents, rotational alignment, steric interlocking, and reduction of free volume due to orientational correlations. Moreover, we know from the work of [3,8], that oblate and prolate maximal packings are not symmetric, and that oblate packing (0.70) is slightly less than prolate (0.71) at its maximal jamming, so ideally the model requires enough flexibility to also capture this.

Symbolic regression is a machine learning method that explores the space of mathematical expressions to find compact closed-form expressions that describe data. In contrast to conventional regression or machine learning methods, where the mathematical structure of the model is assumed a priori, symbolic regression simultaneously searches for both the model's mathematical structure and its optimal parameters. The objective of symbolic regression is to find compact and interpretable expressions that preserve predictive accuracy while keeping the model as parsimonious as possible [20].

To perform SR, we used PySR, which is an open-source framework that relies on evolutionary algorithms to iteratively generate and evaluate candidate mathematical expressions. PySR evaluates a large population of candidate equations and evolves them through mutation and recombination [21]. At each step, equations with lower prediction error are selected while avoiding unnecessary complexity. Finally, a set of possible expressions is proposed by PySR that represents the trade-off between model complexity and goodness of fit. Fig. 2 illustrates the discrepancies between the Yuan et al. [8] baseline model and the benchmark packing data; these discrepancies form the residuals subsequently defined in Eq. (5) and used as the target variable for symbolic regression. We applied SR to the residual packing fraction defined as follows:

$$\eta_{res} = \eta_{data} - \left[C_1 \left(\frac{v_p}{V_{ex}} \right) - C_2 \left(\frac{v_p}{V_{ex}} \right)^2 \right] \tag{5}$$

where η_{data} represents the reference packing fraction obtained from simulation or experimental datasets. The residual term therefore quantifies the component of packing efficiency not captured by the baseline excluded-volume model Eq. (4). The symbolic-regression analysis was conducted using published packing-fraction datasets for spheroidal particles reported by Donev et al. [4] and Yuan et al. [8]. These datasets were used to derive the residual correction term defined in Eq. (5) and should therefore be considered model-development datasets. Subsequent comparisons presented in Figs. 5 and 6 evaluate the ability of the final hybrid model to reproduce these benchmark datasets but do not constitute independent validation.

PySR evaluates candidate expressions using a multi-objective evolutionary search in which equation accuracy and equation complexity are treated as separate objectives. Accuracy was quantified using the mean squared error (MSE) between predicted and observed residual packing fractions. Complexity was measured as the number of expression-tree nodes required to represent an equation, including operators, constants, variables and functions. Rather than combining these objectives into a single score, PySR identifies the Pareto-optimal set of equations for which no simpler equation achieves lower error and no more accurate equation achieves lower complexity. The candidate models reported in Table 1 therefore represent successive points along this Pareto frontier, and the final model was selected at the point where additional complexity yielded diminishing reductions in MSE.

To facilitate the search, we converted the original (v_p/V_{ex}) independent variable to ($x = (V_{ex}/v_p)$-8). Using this change of variable, the residual at α = 1 becomes zero. The transformation $x = (V_{ex}/v_p)$-8 is simply a translation of the predictor variable and does not alter the underlying statistical relationships; it was introduced solely to place the spherical case at the origin and facilitate enforcement of the boundary condition $R(\alpha = 1) = 0$. Additionally, we restricted the fitting domain to aspect ratios $1 \leq \alpha \leq 3.5$, where alignment-induced densification is strongest, and after which no major deviation is observed in computational models. Data at extreme aspect ratios were excluded because the two-term model Eq. (4) already captures the asymptotic behaviour in those regimes. The SR search was configured such that it was allowed to

Table 1
The set of equations found by PySR as possible candidates for $R(\alpha)$ in Eq. (9). Here, x is defined as the exclusion factor minus the exclusion factor of a sphere $x = (\langle V_{ex}(\alpha) \rangle / v_p - 8)$.

Equation number	Complexity	Loss (MSE)	Equation*
T1	1	6.11E-04	0.033
T2	5	4.59E-04	$0.043 - 0.011x$
T3	6	2.27E-04	$xe^{-4.128x}$
T4	7	1.26E-04	$0.143\sqrt{x}e^{-x}$
T5	9	2.00E-05	$0.208\sqrt{xe^{-3.357x}}$
T6	10	8.15E-06	$0.285\sqrt{x}e^{-\sqrt{x}-x}$

use binary operators (+, −, ×) and three unary operators (negation, exp., √). Nested constraints were used to avoid repeated application of the same unary operator. Based on initial evaluations, the maximum expression complexity was set to 11 nodes. The loss function was mean squared error (MSE). To enforce the constraint that the correction vanishes for spheres (x = 0), the origin point (x = 0, η_{res} = 0) was included as a soft constraint in the symbolic-regression loss function by assigning it a weight of 3.

2.4. Friction

Interparticle friction profoundly influences the packing of spheroidal particles by restricting the translational and rotational rearrangements required to achieve efficient local configurations. In the frictionless limit, particles can readily reorient and develop orientational correlations that promote dense packing, whereas increasing friction progressively inhibits these rearrangements, producing a smooth transition from random close packing (RCP) to random loose packing (RLP) as the friction coefficient μ increases [7]. In the frictionless limit ($\mu = 0$), particles enjoy full rotational freedom and can collectively align to maximize packing density, achieving the high-volume-fraction RCP state [4]. By contrast, at very large friction ($\mu \to \infty$), rotational degrees of freedom are essentially frozen out, eliminating alignment correlations and orientational entropy effects. The packing then converges to the RLP regime characterized by minimal structural correlations and a packing fraction governed almost solely by excluded-volume constraints. In other words, increasing friction progressively suppresses the alignment-based densification that nonspherical particles would otherwise gain from orientational order, while leaving the baseline excluded-volume contribution to packing density intact. Packings at intermediate friction can be viewed as perturbations around the frictionless RCP state, developing modest local orientational correlations and progressively lower densities until friction becomes large enough to suppress these correlations entirely in the RLP state. This picture, demonstrated by Yuan et al. (2021) and [7], unifies frictional packings by showing that friction effectively tunes the system between two extremal states: maximally correlated, dense RCP (no friction) and uncorrelated, loose RLP (infinite friction).

To interpolate between the random loose packing (RLP) and random close packing (RCP) limits in granular media, we implemented the friction-dependent master curve proposed by Yuan et al. (2021). This approach provides a physically grounded framework for capturing the continuous transition in packing fraction as a function of interparticle friction, μ, and is particularly well-suited for modelling the behaviour of disordered packings across a range of particle shapes and frictional conditions. The master curve is defined by a logistic function that describes the normalized packing fraction as a function of μ:

$$f(\mu) = \frac{1}{1 + (\mu/\mu^*)^{\Omega}} \tag{6}$$

where $\mu^* = 0.1636$ is the characteristic friction scale and $\Omega = 1.07$ is the logistic exponent. This function satisfies the boundary conditions $f(0) = 1$ (frictionless RCP) and $f(\mu \to \infty) = 0$ (high-friction RLP), and has been shown to collapse packing data from a wide range of particle shapes onto a single curve when normalized appropriately [8]. We used this friction factor to interpolate the coefficients C_1 and C_2 in Eq. (4). The coefficients C_1 and C_2 were interpolated as:

$$C_1(\mu) = C_1^{RLP} + f(\mu)\left(C_1^{RCP} - C_1^{RLP}\right) \tag{7}$$

$$C_2(\mu) = C_2^{RLP} + f(\mu)\left(C_2^{RCP} - C_2^{RLP}\right) \tag{8}$$

With $C_1^{RLP} = 7.465$, $C_1^{RCP} = 13.499$, $C_2^{RLP} = 24.522$, $C_2^{RCP} = 67.034$ based on empirical fits to the RLP (0.55) and RCP (0.64) for spheres and reproducing Yuan, Jiao, Wang and Li [8] within rounding. This formulation ensures that the model captures the nonlinear, monotonic decrease in packing efficiency with increasing friction, while preserving the known asymptotic behaviours at both frictional extremes.

Fig. 3 illustrates the friction-dependent evolution of the empirical coefficients C_1 and C_2 in the excluded-volume-based packing model, as governed by the logistic master curve of Yuan, Jiao, Wang and Li [8]. The results show that both coefficients decrease monotonically with increasing friction coefficient (μ), reflecting the progressive suppression of contact number (C_1) and higher-order structural correlations (C_2) as the system transitions from the frictionless random close packing (RCP) regime to the high-friction random loose packing (RLP) limit. This behaviour highlights the importance of incorporating friction-dependent interpolation into packing models to accurately capture the physical mechanisms that govern particle arrangement and porosity across a range of granular systems. Moreover, Using the friction-interpolated coefficients Eqs. (7)–(8), the baseline model reproduces the packing-fraction master curve reported by Yuan et al. [8] for frictional packings, thereby providing a continuous interpolation between the published RLP and RCP limits.

2.5. Dense packing in spheroids that are close to spheres

To address the underprediction of dense packing in spheroids with aspect ratios near unity, we extended the Yuan, Jiao, Wang and Li [8] model by incorporating an additional term that accounts for rotational alignment effects. While the original model captures the excluded-volume-driven behaviour of frictional packings, it does not fully represent the enhanced packing efficiency observed in nearly spherical particles due to their ability to align and reduce local excluded volume. To capture this effect, we introduced a rotational alignment correction term, $R(\alpha)$, modulated by $f(\mu)$ with the increasing friction suppressing the rotational alignment of the particles in the orientation averaged packing. The excluded-volume and frictional components are physically motivated, whereas this rotational correction term $R(\alpha)$ should be interpreted as an empirically derived closure which we obtain through symbolic regression. The modified packing fraction model is expressed as:

$$\eta(\alpha,\mu) = C_1(\mu)\frac{v_p}{\langle V_{ex}(\alpha)\rangle} - C_2(\mu)\left(\frac{v_p}{\langle V_{ex}(\alpha)\rangle}\right)^2 + f(\mu)(R(\alpha)) \tag{9}$$

The first two terms capture the baseline response, now adjusted for friction through Eqs. (7) & (8). These describe the behaviour of the packing as a function of friction through the master curve of Yuan, Jiao, Wang and Li [8]. The third term ($R(\alpha)$, addressed below) is a function that represents rotational freedom that changes with exclusion fraction which is a function of α. We also assume (via multiplying by $f(\mu)$) that rotational freedom of particles follows the friction master curve Eq. (6), ensuring that alignment-driven densification contributes fully only to the frictionless limit $f(\mu = 0)$ and vanishes as $f(\mu \to \infty)$.

To ensure physically meaningful behaviour, we imposed explicit boundary conditions on the correction term and frictional scaling. First, the rotational-alignment contribution must vanish for spheres, which do not exhibit alignment-induced densification; therefore we enforce $R(\alpha = 1) = 0$ Eq. (9) by defining the symbolic regression variable as $x = (V_{ex}/v_p - 8)$, where 8 is the excluded-volume factor of a sphere. Second, the friction master curve satisfies $f(0) = 1$ (full alignment in the frictionless RCP limit) and $f(\mu \to \infty) = 0$ (no alignment in the high-friction RLP limit), ensuring a smooth transition between the two physical extremes. Third, because $V_{ex}/v_p \to \infty$ as $\alpha \to 0$ or $\alpha \to \infty$, Eq. (9) correctly yields $\eta \to 0$ for highly oblate or prolate shapes. This excluded-volume scaling therefore applies rigorously to the infinite-friction ($\mu \to \infty$) RLP state for all particle shapes. In the frictionless limit, excluded-volume control is recovered only for extremely oblate or prolate particles, where geometric constraints eliminate the orientational correlations responsible for near-sphere densification. Finally, the chosen coefficients reproduce the known spherical limits $\eta = 0.64$ (RCP)

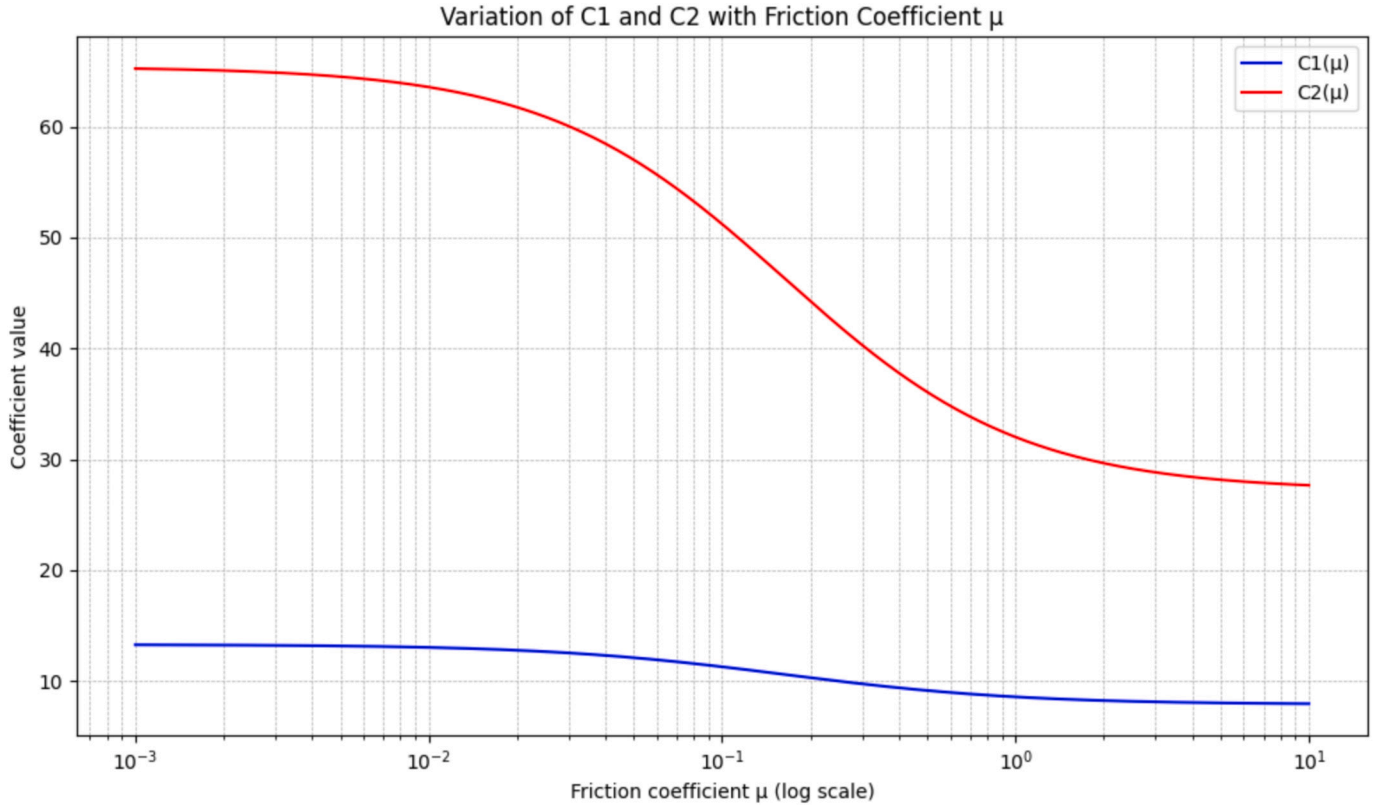


Fig. 3. Variation of the excluded-volume model coefficients C_1 and C_2 as a function of the interparticle friction coefficient (μ), plotted on a logarithmic scale. The coefficients are interpolated using the logistic master curve of Yuan, Jiao, Wang and Li [8], with parameters $\mu^* = 0.1636$ and $\Omega = 1.07$.

and $\eta = 0.55$ (RLP), anchoring the model to well-established experimental benchmarks.

2.6. Hybrid model formulation and symbolic regression results

Table 1 reports the set of equations identified by PySR for the term $R(\alpha)$ together with their corresponding loss values (MSE), which provide an indication of the goodness of fit to the residuals, η_{res}. The functional forms of all candidate equations are illustrated in Fig. 4. As expected, the MSE generally decreases with increasing model complexity. However, this decrease is not uniform and a significant drop in MSE can be observed between Equation number T4 and T5, where the MSE decreases from 1.26E-04 to 2.00E-05. This point marks the transition where a slight increase in the model complexity leads to a substantial reduction in the residuals while for greater complexities has negligible effect on the model fit. As a result, we select equation number T5, with a complexity of 9, as $R(\alpha)$ in Eq. (9). Moreover, Equation T5 was selected because it corresponds to the elbow of the Pareto frontier, where model error decreases by more than a factor of six relative to T4 while requiring only a modest increase in complexity. Subsequent increases in complexity produced comparatively small improvements in MSE, indicating diminishing returns. The exact expression returned by PySR was $R(x) = P\left(xe^{-3.357x}\right)^{1/2}$. For incorporation into the final packing model, the expression was simplified by expanding the square root to give $R(x) = P\sqrt{x}e^{-1.6785x}$, and then approximating the exponential coefficient 1.6785 by the rational value 5/3. The resulting closed-form approximation was $R(x) \approx P\sqrt{x}e^{-5x/3}$, while allowing the amplitude coefficient to be recalibrated separately for prolate and oblate spheroids. This simplification preserves the unimodal shape and rapid decay behaviour of the symbolic-regression solution while improving interpretability and facilitating implementation. The resulting approximation is:

$$R(\alpha) = P\left(\sqrt{\frac{\langle V_{ex}(\alpha)\rangle}{v_p} - 8}\right)\exp\left[-\frac{5}{3}\left(\frac{\langle V_{ex}(\alpha)\rangle}{v_p} - 8\right)\right] \tag{10}$$

where the best-fitted P values that yield the peak are $P = 0.190$ for prolate and $P = 0.175$ for oblate. The friction master curve Eq. (6) then multiplies $R(\alpha)$ interpolating the packing fraction between the RLP and RCP limits.

Hence, the most suitable model for packing fraction found was Eq. (9) using $R(\alpha)$ Eq. (10) with the values of C_1 Eq. (7) and C_2 (Eq. (8) depending on friction Eq. (6) matching the simulation data of Donev, Cisse, Sachs, Variano, Stillinger, Connelly, Torquato and Chaikin [4,8] for orientation averaged spheroids. Here, orientation averaging refers to an ensemble average over all relative particle orientations when computing the excluded volume and packing statistics. The resulting packing is assumed to be macroscopically isotropic, such that any local or transient orientational ordering averages out at the bulk scale, with no preferred fabric direction.

3. Results

3.1. Model output

Fig. 5 illustrates the model output and how the predicted packing fraction varies with particle aspect ratio for different values of the friction-dependent packing between RLP and RCP. The horizontal axis spans a wide range of aspect ratios on a logarithmic scale, from highly oblate ($\alpha \ll 1$) to highly prolate ($\alpha \gg 1$) shapes. Each curve corresponds to a specified friction coefficient, μ, with lower μ permitting a larger contribution from the alignment correction and therefore producing greater near-sphere densification. Except in the infinite-friction limit, the curves exhibit two packing maxima close to, but on either side of, $\alpha = 1$: one for moderately oblate spheroids and one for moderately

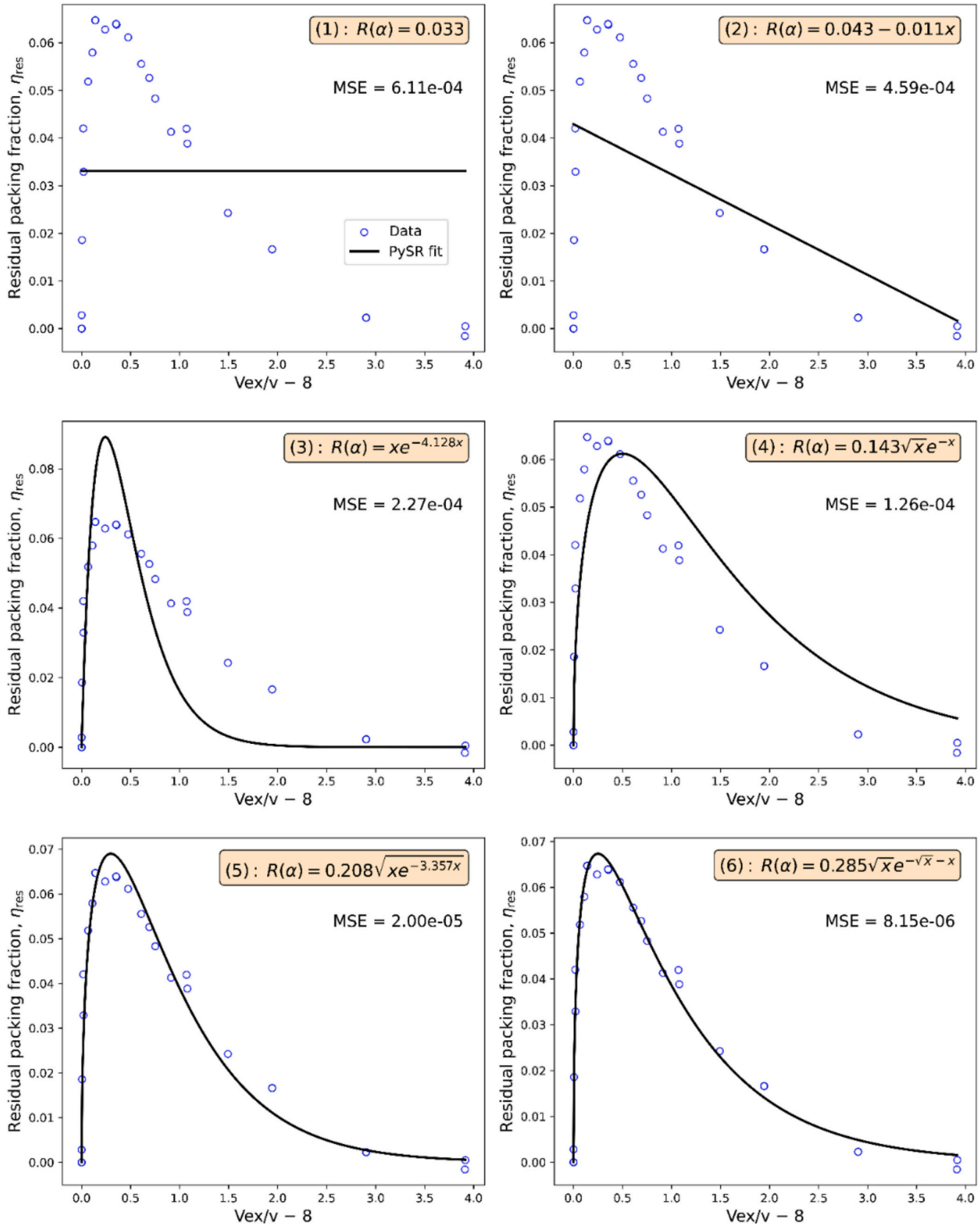


Fig. 4. Mathematical empirical expressions found by PySR for modelling the residual packing fraction, η_{res}, in Eq. (5).

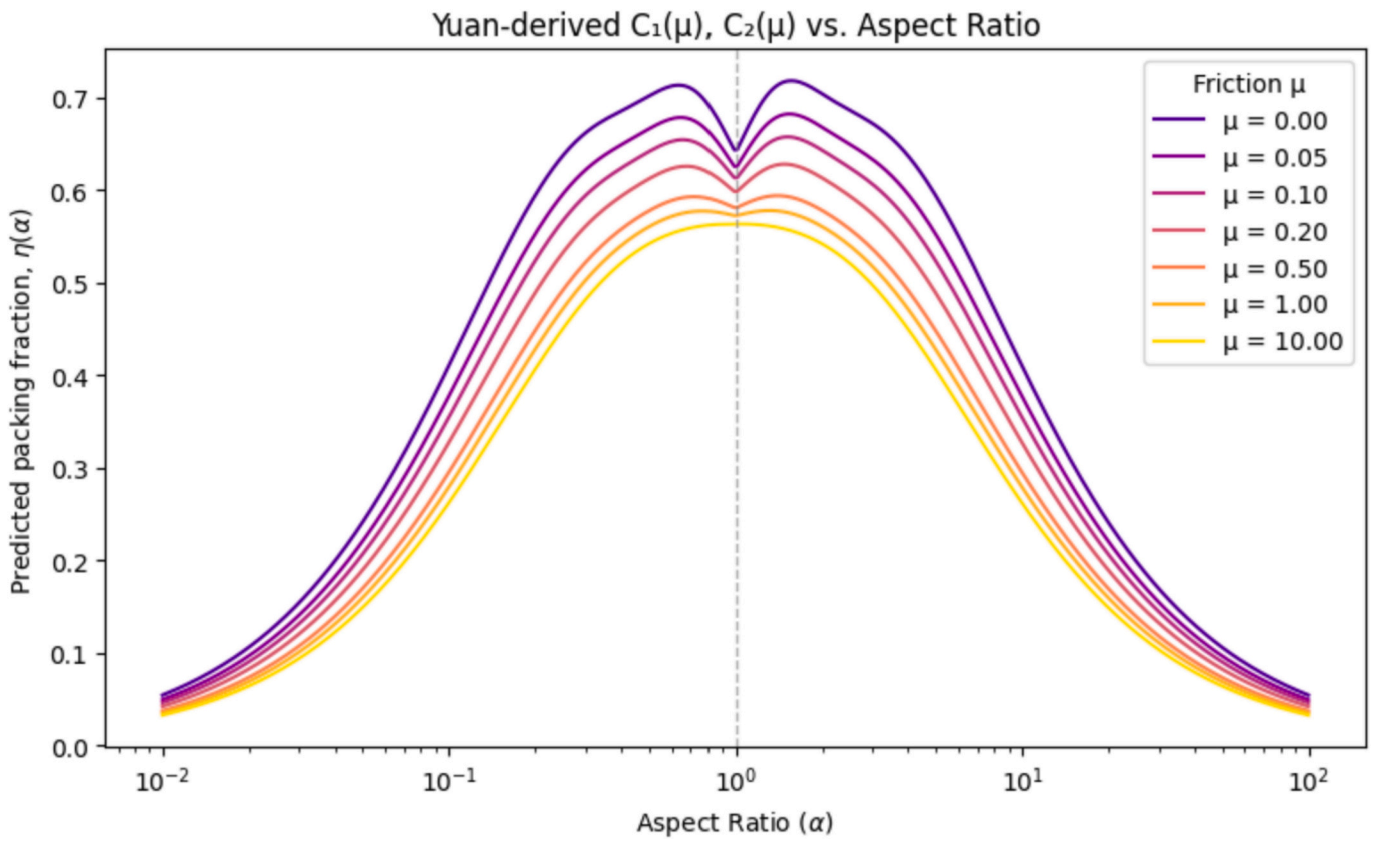


Fig. 5. Predicted packing fraction as a function of particle aspect ratio (AR), generated using the new friction-dependent master equation Eq. (9). Each curve corresponds to a different value of friction coefficient resulting in packing fractions smoothly interpolated from 0.55 to 0.64 for spheres, illustrating how decreasing friction systematically raises the predicted packing fraction across all aspect ratios. The vertical dashed line at $\alpha = 1$ marks the spherical case.

prolate spheroids. The spherical geometry at $\alpha = 1$ forms a local minimum between these maxima because slight departures from sphericity introduce additional effective rotational degrees of freedom (from 3 of a sphere to 5 of a spheroid) and enable more efficient local packing arrangements. As particles become moderately oblate or prolate, enhanced orientational flexibility promotes local alignment and nesting, increasing packing density. However, beyond the optimal aspect ratio, these benefits are progressively outweighed by the rapid increase in excluded volume and geometric frustration associated with highly elongated or flattened particles. Consequently, packing fraction declines toward both aspect-ratio extremes. The model also reproduces the slightly lower maximum packing fraction of oblates relative to prolates, consistent with numerical studies [3,8].

3.2. Model performance

The proposed packing model reproduces the benchmark experimental and simulation datasets used for model development and comparison across a broad range of aspect ratios, faithfully reproducing the known non-monotonic packing trends from sphere to spheroid geometries. In Fig. 6, model predictions (coloured curves) closely track simulation and experimental results over several orders of magnitude in aspect ratio. Notably, the model captures the dip in packing efficiency at perfect sphericity ($\alpha = 1$) and the subsequent increase in packing fraction as particles become moderately aspherical, reaching a peak density at intermediate aspect ratios ($\sim\alpha$ 1.5 for prolate and $\sim$0.67 for oblate spheroids). This behaviour is tailored to the simulations by Donev, Cisse, Sachs, Variano, Stillinger, Connelly, Torquato and Chaikin [4] who reported maximal random close packing fractions of $\sim$0.70 for oblate and $-$ 0.71 for prolate spheroids. Likewise, the model's predictions align with the experimental data of [5,6,22] for ellipsoids (showing similar densification at moderate asphericity) and the numerical results of [8], showing close agreement with the benchmark datasets from across the RLP–RCP spectrum (grey diamonds). In all cases, the predicted packing fractions remain within the expected random loose packing ($\sim$0.55) to random close packing ($\sim$0.64) limits for frictional spheres, indicating that the model faithfully adheres to known physical bounds while still capturing shape-specific effects.

Importantly, the model also reproduces the qualitative packing trends observed across particle shapes—including the increase in porosity when transitioning from spheres to more extreme spheroids. While moderate deviations from unity aspect ratio allow particles to nest and orient more efficiently (reducing porosity), at high aspect ratios the packing fraction drops off sharply due to growing excluded volume and steric hindrance. The model predicts this steep decline in density for both needle-like prolates and disk-like oblates, consistent with the high porosities reported in simulations and experiments for extreme shapes (e.g., packing fractions falling well below that of spheres). This outcome matches the universal packing trend noted by [5,6,16,22] – namely, that beyond a certain point, increasing particle asphericity leads to disproportionately larger void space and hence lower bulk density. Compared to earlier analytical approaches, the new model offers a notable improvement in fidelity. Previous excluded-volume models (e.g., mean-field or two-term fits) tended to systematically under-predict the densification near spherical shapes and could not reproduce the subtle asymmetry between prolate and oblate packing maxima. By incorporating a shape-dependent rotational freedom term, $R(\alpha)$, our model remedies these issues: it captures the near-sphere packing enhancement and the slight prolate–oblate difference (prolate spheroids packing marginally denser packings than oblates at the optimal aspect ratio, as observed by [3,8]). This refinement, which was anticipated by Robinson, Friedman, Thomas, Hirmas, Sullivan and Nemes [9], builds upon

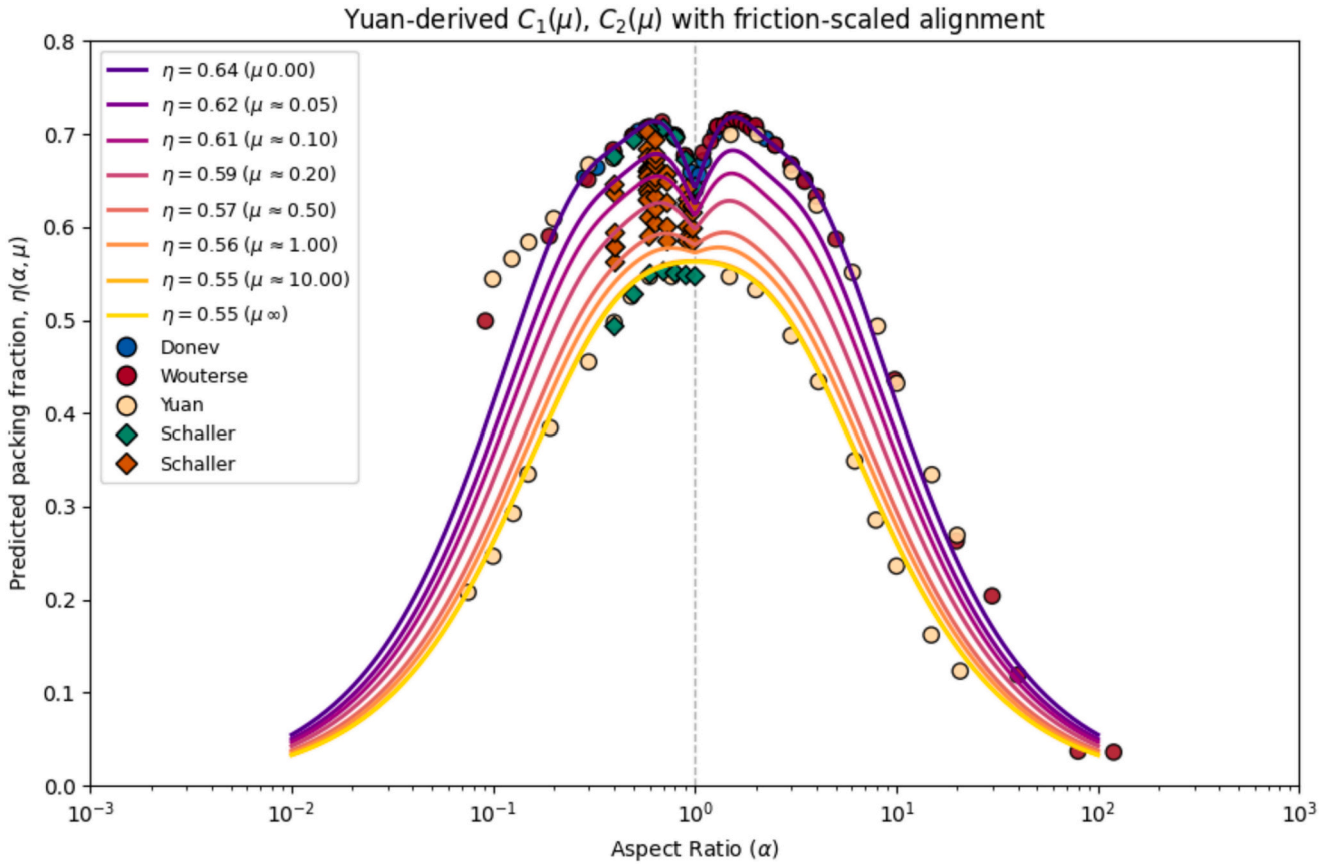


Fig. 6. Predicted packing fraction as a function of spheroid aspect ratio, generated using Eq. (9). Coloured curves represent model predictions for different friction coefficients. Symbols show the published datasets used for model development and comparison, as identified in the legend, blue [4], red [6], and yellow [8] and the diamonds the data of [23]. The vertical dashed line denotes the spherical limit, α = 1. (For interpretation of the references to colour in this figure legend, the reader is referred to the web version of this article.)

the framework of Yuan, Jiao, Wang and Li [8] and ensures accurate performance from the needle-like and disk-like extremes to the spherical case.

The new friction-dependent master equation provides a complementary but fundamentally different description of nonspherical particle packing compared with the results of the Delaney, Hilton and Cleary [7] sedimentation-based simulations. Delaney's approach derives packing fractions from gravitational settling of frictional and frictionless prolate particles with different aspect ratios, under Stokes drag, assuming a liquid phase with different viscosities. Particles progressively align as they sediment, producing an orientation distribution strongly biased toward parallel alignment for zero friction and random orientation for high friction. As a result, the reported packing fractions reflect a directionally constrained microstructure, in which end-on (edge-to-face) and face-on contact geometries occur with unequal probability and the packing state is shaped by hydrodynamic alignment pathways during descent. By contrast, the proposed model adopts an orientation-averaged excluded-volume representation, integrating over the full space of spheroid orientations rather than imposing a mechanically or hydrodynamically favoured alignment. This produces packing predictions representative of a statistically isotropic ensemble of spheroids, relevant to frictional jamming, granular agitation, and disordered preparation protocols that do not impose directional settling. Consequently, while Delaney's simulations capture the packing fraction attainable under sedimentation-induced alignment—typically yielding higher packing density where parallel alignment reduces excluded volume, as indicated by the dashed black line in Fig. 7 that represents simple cubic aligned spheroids—the new model predicts the ensemble-mean packing fraction arising when all relative orientations contribute according to their geometric weighting. The simulations drop below the orientation averaged model for RLP, in agreement with Delaney's conceptual diagram of edge-to-face packing, because sedimentation induces alignment that reduces packing efficiency under high friction. The RCP data follow the orientation averaged model and not a straight line, suggesting they don't follow Delaney's conceptual aligned model, but have in fact 'average' orientation. The contrast between the two, especially at RLP, thus reflects their different physical assumptions: Delaney's model quantifies a process-specific packing state dominated by alignment during settling, whereas Eq. (9) quantifies a shape-controlled mean-field-like state appropriate for a frictional range of orientation-disordered packings. Together, they potentially delineate the upper and lower levels associated with the packing process, indicating how alignment state mediates the packing efficiency of spheroids. In this case, the comparison represents sedimentation; compaction would shift the responses in the directions shown by the black and grey arrows as dependent on the packing alignment.

A further point of validation comes from comparison with the analysis of [24] for the dielectric and electrical-conductivity behaviour of densely packed sands. In that work, coarse quartz sand was shown to behave as if composed of oblate spheroidal grains with an effective aspect ratio of approximately 0.46, a shape required to replicate the observed permittivity and electrical response of the material. For such sands, [24] reported a maximum packing fraction close to 0.64, consistent with dense but friction-limited grain contacts. Using a representative interparticle friction coefficient of $\mu \approx 0.1$—appropriate for quartz sand and well supported by independent measurements of quartz-dominated sandstones, which typically exhibit static friction values of $\mu \approx 0.1$–0.2 [25]—Eq. (9) of the present model predicts a

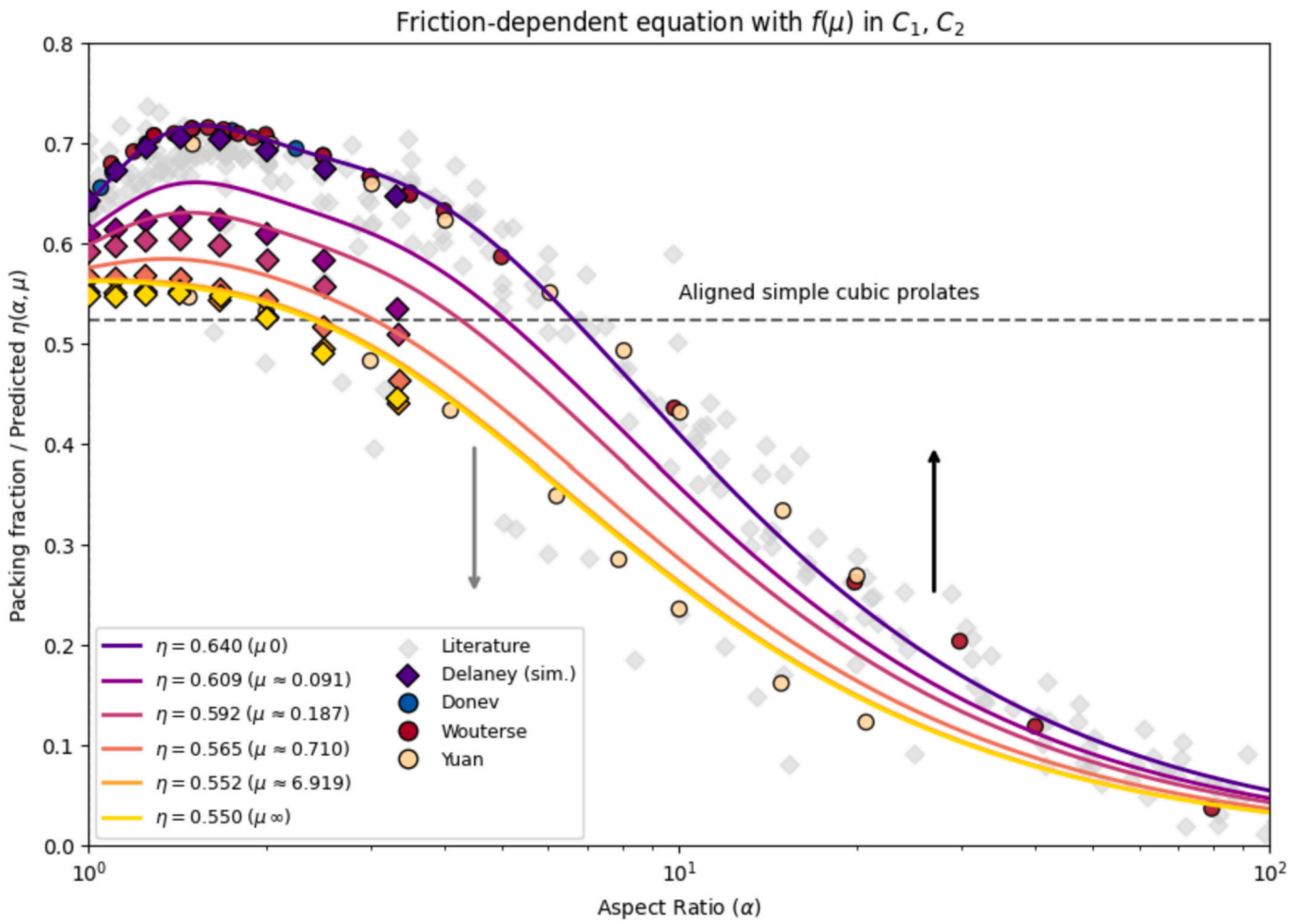


Fig. 7. Predicted packing fraction as a function of particle aspect ratio (α), generated using Eq. (9). The coloured model curves represent orientation-averaged spheroids, each corresponding to a different target packing fraction (η = 0.55–0.64 for spheres). Coloured diamond markers show the Delaney, Hilton and Cleary [7] simulation data for sedimented particles, with each Delaney point coloured to match the corresponding η-curve in the model. Circular markers show additional experimental and simulation results: blue [4], red [6], and yellow [8] and grey markers literature data. The black dashed horizontal line denotes the packing fraction for simple-cubic arrangements of perfectly aligned spheroids (cos γ = 1). The black arrow indicates the direction the orientation-averaged model curves would shift under perfect parallel alignment, whereas the grey arrow shows the shift expected for perpendicular alignment (cos γ = 0). (For interpretation of the references to colour in this figure legend, the reader is referred to the web version of this article.)

packing fraction of $\eta = 0.635$ for an oblate particle with aspect ratio $\alpha = 0.46$. The correspondence suggests that $\mu \approx 0.1$ may provide a useful illustrative value for coarse quartz-dominated sands within the present model. However, this value should not be regarded as universally applicable because effective friction depends on particle roughness, morphology, contact conditions and preparation history; in time this is something open to further research, This close correspondence demonstrates that the hybrid packing framework not only captures numerical and experimental trends but also reproduces empirically inferred shape–friction combinations derived from independent physical property measurements.

4. Discussion

The physically-informed nature of the model yields clear insight into how particle shape and excluded volume govern packing behaviour. By explicitly incorporating the orientation-averaged excluded volume, the model reveals a non-monotonic packing efficiency as aspect ratio deviates from unity, reflecting two competing mechanisms. At moderate asphericity for spheroids, and for asphericity more generally, additional rotational degrees of freedom allow particles to orient and nest more efficiently, temporarily increasing the packing fraction above that of spheres. This aligns with simulations by Donev, Cisse, Sachs, Variano, Stillinger, Connelly, Torquato and Chaikin [4], who showed that slightly elongated or flattened particles (aspect ratios ~1.5 for prolates or ~0.67 for oblates) can attain packing fractions around 0.68–0.71, outperforming random close-packed spheres (~0.64). The model reproduces this shape-induced densification by capturing how moderate asphericity reduces void space via orientational alignment. However, as the aspect ratio becomes extreme (highly prolate or highly oblate), the relative excluded volume (V_{ex}/v_p) increases rapidly — scaling ∝ aspect ratio for rods and ∝ 1/aspect ratio for disks — severely limiting the number of neighbours a particle can accommodate. The model predicts a corresponding decline in packing fraction at extreme aspect ratios, approaching the highly porous limits observed in experiments and simulations (packing fractions dropping well below 0.2 for the most elongated/flattened shapes) (Fig. 6). In essence, the initial rise in density is driven by shape-enhanced packing (an entropic effect of orientational freedom), whereas the eventual drop is dictated by steric exclusion – a mechanistic interpretation consistent with the theoretical framework of excluded-volume dominated packing. This explanation, grounded in geometry, goes beyond statistical correlations by directly linking particle morphology to bulk porosity and effectively identifies spherical particles as a local packing-efficiency minimum rather than a maximum.

Our formulation follows Yuan, Jiao, Wang and Li [8] in treating the infinite-friction, RLP regime as a monotonic excluded-volume baseline across shapes, and finite friction as a perturbation away from that state. To reproduce the near-sphere density enhancement observed under low friction / frictionless conditions, we add a shape-dependent alignment term $R(\alpha)$ that is scaled by the frictional master curve Eq. (6). This separation clarifies that Yuan's RLP scaling does not by itself generate the near-sphere non-monotonic peak; the peak emerges when orientational correlations become active as friction decreases.

Beyond matching empirical trends, the model captures emergent behaviours that eluded earlier statistical models, offering a unified physical interpretation. Our model's additional shape-dependent alignment term $R(\alpha)$ (corresponding to orientational ordering effects) reproduces the near-sphere density peaks and the subtle asymmetry between prolate and oblate packings. Notably, simulations have shown that prolate spheroids jam slightly more densely (peak $\eta \approx 0.71$) than their oblate counterparts (peak $\eta \approx 0.70$) [3]. The inclusion of $R(\alpha)$ further extends the model's predictive power: as Robinson, Friedman, Thomas, Hirmas, Sullivan and Nemes [9] posited, incorporating a term that vanishes at infinite friction and is fully active at zero friction allows a smooth transition between the random loose and random close packing limits. Indeed, in the high-friction (RLP) regime, the model reduces to a simple excluded-volume control of density (consistent with Yuan et al.'s finding that RLP packings obey a monotonic excluded-volume scaling). In the frictionless limit, it recovers the alignment-driven densification noted above, matching the maximal packings reported by Donev [3] and others. Wouterse, Williams and Philipse [6] and colleagues had experimentally confirmed this counter-intuitive trend – a shape-dependent density maximum – in colloidal ellipsoid packings, something unattainable with earlier mean-field models. By embedding the physics of exclusion, orientation, and frictional constraints into the closed-form model formulation, the present model not only fits the data but also illuminates the underlying causes of packing variation. The model shows that friction vertically modulates how much of the shape-dependent alignment term contributes to packing: reducing friction allows alignment-induced densification to emerge, while increasing friction suppresses it, leaving the packing governed primarily by the friction-independent excluded-volume baseline. Such mechanistic insights – for example, recognizing that friction tunes the system continuously between an uncorrelated, low-density state and an alignment-supported dense state – were largely absent from purely empirical or statistical descriptions. In summary, the model translates complex packing phenomena into interpretable parameters, demonstrating how particle shape (aspect ratio), excluded volume, and interparticle friction together dictate the attainable packing fraction and porosity, in agreement with both classical packing theory and contemporary observations.

The hybrid packing model developed in this study provides a physically grounded yet computationally efficient framework for predicting the packing behaviour of granular materials containing non-spherical particles. By combining excluded-volume theory, friction-dependent packing transitions, and a symbolic-regression-derived rotational correction, the model links particle-scale geometry and contact mechanics to macroscopic packing fraction across a wide range of spheroidal particle shapes. In doing so, it offers a tractable alternative to computationally intensive numerical simulations while retaining a clear connection to the underlying physics governing jammed packings and granular structure.

Recent advances in real-particle packing research have increasingly relied on physics-engine and discrete-element-based simulations to represent complex particle geometries, particle-size distributions, and contact interactions. For example, three-dimensional digitalization and physics-engine approaches have been used to reproduce the packing behaviour of realistic recycled aggregates, demonstrating the importance of particle morphology and contact mechanics in determining packing structure and density [26]. Similarly, studies of recycled fine aggregates have shown that interparticle friction, particle arrangement, and packing state strongly influence rheological behaviour and workability [27], while mixed particle-size distributions and irregular particle shapes can substantially modify packing efficiency relative to idealized systems [28]. These studies highlight factors that are not resolved explicitly in the present framework. Rather than modelling individual particle contacts or detailed packing protocols, the proposed model provides a reduced-order analytical description that captures the first-order influences of particle shape and friction through orientation-averaged excluded-volume relationships. Consequently, the framework should be viewed as complementary to detailed numerical simulations: it sacrifices geometric realism and particle-scale resolution in exchange for computational efficiency, physical interpretability, and rapid prediction across a broad range of spheroidal particle shapes. Extension of the approach to account for particle angularity, broad size distributions, and more complex contact laws represents a promising direction for future work.

Beyond its relevance to granular physics and powder technology, the model also provides a useful bridge to Earth-system applications and other planets [29], where soils, sediments, regoliths and other unconsolidated materials can be viewed as granular assemblies whose bulk properties emerge from particle-scale packing processes [30–32]. The ability of the model to reproduce the non-monotonic relationship between aspect ratio and packing fraction suggests a pathway toward improved mechanistic understanding of how particle morphology influences bulk density, porosity, permeability and compaction behaviour in natural materials. Such links are particularly valuable because they provide a common conceptual framework through which observations from granular physics can be translated into practical interpretations of sediment structure, soil architecture and porous-media behaviour. More broadly, the model highlights how relatively small changes in particle morphology can propagate across scales to influence pore-network geometry, hydraulic conductivity, gas diffusion, mechanical stability and susceptibility to densification under external loading. In soils and sediments, where particle shape varies as a consequence of weathering, transport and aggregation processes, these effects may contribute to systematic differences in bulk density and pore connectivity that are often treated empirically [33]. By explicitly linking aspect ratio, friction and packing state, the proposed framework offers a physically interpretable basis for investigating how mineral grains, biogenic particles, aggregates and fragmented materials organize into larger-scale structures. This may provide a useful foundation for future efforts to couple granular packing theory with pedophysical, hydrogeological and geomorphological models, ultimately helping to explain how particle-scale morphology influences water retention, infiltration, aeration, root penetration and sediment transport behaviour across a wide range of environmental systems. These links are increasingly recognised within soil science and sedimentology, where bulk density, porosity and permeability are now viewed as emergent properties of pore geometries generated by particle packing and morphology [9,34]. Particle shape has been shown to influence pore-throat size distributions, water-retention characteristics, permeability and fluid transport pathways in both soils and sediments [35,36], suggesting that analytical packing models may provide a valuable mechanistic bridge between granular-scale physics and larger-scale geomorphic, hydrological and pedological processes.

Compared with purely empirical correlations, the present formulation offers greater physical interpretability, while avoiding the computational expense and protocol dependence associated with large-scale DEM or molecular-dynamics simulations. Nevertheless, several important limitations remain. The current model assumes monodisperse, isotropic assemblies of ideal spheroids and does not account for particle-size distributions, angular or irregular particle geometries, or cohesive interactions. Surface forces such as van der Waals attraction, electrostatic interactions and capillary bonding become increasingly important for fine-grained materials, particularly clay-rich systems where these

forces may dominate over gravitational effects [37,38]. Furthermore, natural and industrial granular materials commonly exhibit anisotropic fabrics, multimodal size distributions and mixed particle morphologies that fall outside the assumptions of the present framework. Moreover, although the model reproduces multiple published experimental and simulation datasets, most available spheroidal packing datasets are limited in number and were also used during model development. Consequently, the current study should be viewed as demonstrating consistency with established benchmark data rather than providing a fully independent validation.

Future work should evaluate the framework against new experimental datasets spanning broader particle shapes, friction coefficients and preparation protocols. In addition, focus on extending the model to polydisperse systems, mixtures of particle shapes, stress-dependent fabric evolution and orientation-dependent packing states, including nematic and partially ordered structures could be undertaken. Such extensions would provide a closer connection between analytical packing theory and the complexity of real granular materials, while preserving the interpretability and efficiency that make hybrid analytical approaches attractive. Ultimately, the framework presented here may serve as a foundation for a new generation of physically informed packing models that bridge fundamental granular mechanics with practical applications in powders, sediments, soils and other porous particulate media.

5. Conclusions

This study presents a friction-dependent analytical model for predicting the packing fraction of isotropically packed spheroidal particles across a wide range of aspect ratios and packing states. Building on the excluded-volume framework of Yuan et al. [8], the model introduces a symbolic-regression-derived rotational correction that captures the characteristic densification peak observed near spherical geometries while preserving the physically constrained behaviour at extreme aspect ratios.

The proposed formulation provides a compact hybrid description of spheroidal particle packings by combining excluded-volume physics, friction-dependent packing transitions and an empirical closure representing orientational packing effects. The model successfully reproduces key features reported in numerical and experimental studies, including the non-monotonic dependence of packing fraction on aspect ratio, the transition between random loose and random close packing limits, and the subtle asymmetry between oblate and prolate spheroids. These results demonstrate that a substantial proportion of the observed packing behaviour can be captured within a simple analytical framework without recourse to computationally intensive simulations.

More broadly, the study demonstrates the potential of symbolic regression as a tool for discovering compact empirical closed-form corrections to established physical models. Rather than replacing mechanistic theory, the symbolic-regression approach complements existing excluded-volume formulations by identifying interpretable closure terms that account for unresolved packing behaviour. This provides a promising pathway for developing analytical models that retain physical transparency while reproducing increasingly complex features of granular systems.

The model is intended primarily as a framework for understanding and predicting the packing behaviour of anisotropic granular materials. However, because particle packing fundamentally controls porosity, bulk density and transport properties, the formulation also provides a bridge between granular physics and application domains including powders, sediments, soils and other particulate porous media. By linking particle-scale geometry and friction to macroscopic packing behaviour, the model offers a foundation for developing more physically based descriptions of natural and engineered granular systems.

Several limitations remain. The current formulation assumes monodisperse, statistically isotropic assemblies of ideal spheroids and does not incorporate particle-size distributions, particle angularity, cohesive interactions, or fabric anisotropy associated with preferred particle orientations. The alignment term included in the model represents local orientation-dependent packing correlations under isotropic conditions, rather than the development of a directional packing fabric. Future developments should therefore focus on extending the framework to anisotropic orientation distributions, fabric evolution under stress, and ordered or partially ordered packing states.

CRediT authorship contribution statement

David A. Robinson: Writing – original draft, Funding acquisition, Formal analysis, Conceptualization. **Sarem Norouzi:** Writing – review & editing, Methodology, Formal analysis. **Amy Thomas:** Writing – review & editing. **Lis Wollesen de Jonge:** Writing – review & editing, Funding acquisition. **Shmulik P. Friedman:** Writing – review & editing, Conceptualization.

Disclosure

Work funded by the European Union. Views and opinions expressed are, however, those of the authors only and do not necessarily reflect those of the European Union or the Research Executive Agency. Neither the European Union nor the granting authority can be held responsible for them.

Declaration of generative AI and AI-assisted technologies in the writing process

Any use of generative AI in this manuscript adheres to ethical guidelines for use and acknowledgement of generative AI in academic research. Each author has made a substantial contribution to the work, which has been thoroughly vetted for accuracy, and assumes responsibility for the integrity of their contributions. During the preparation of this work the author used copilot for paragraph and sentence structuring in order to improve the consistency of the language across multiple international authors. After using this tool, the authors reviewed and edited the content as needed and take full responsibility for the content of the publication.

Declaration of competing interest

The authors declare that they have no known competing financial interests or personal relationships that could have appeared to influence the work reported in this paper.

Acknowledgments

Funding: This project acknowledges funding from the European Union's Horizon Europe research and innovation program under grant agreement No.-101086179; and funding from the UK Research and Innovation (UKRI) under the UK government's Horizon Europe funding guarantee [grant number 10053484] as part of AI4SoilHealth. The Research Council of Norway, Climasoil, Project number: 325253.

Appendix A. Supplementary data

Supplementary data to this article can be found online at https://doi.org/10.1016/j.powtec.2026.123424.

Data availability

All the data was taken from the literature and is published

References

[1] S. Torquato, F.H. Stillinger, Jammed hard-particle packings: from Kepler to Bernal and beyond, Rev. Mod. Phys. 82 (2010) 2633.
[2] A. Baule, H.A. Makse, Fundamental challenges in packing problems: from spherical to non-spherical particles, Soft Matter 10 (2014) 4423–4429.
[3] A. Donev, PhD Jammed Packings of Hard Particles, Princeton University, 2006.
[4] A. Donev, I. Cisse, D. Sachs, E.A. Variano, F.H. Stillinger, R. Connelly, S. Torquato, P.M. Chaikin, Improving the density of jammed disordered packings using ellipsoids, Science 303 (2004) 990–993.
[5] S.R. Williams, A.P. Philipse, Random packings of spheres and spherocylinders simulated by mechanical contraction, Phys. Rev. E 67 (2003) 051301.
[6] A. Wouterse, S.R. Williams, A.P. Philipse, Effect of particle shape on the density and microstructure of random packings, J. Phys. Condens. Matter 19 (2007) 406215.
[7] G.W. Delaney, J.E. Hilton, P.W. Cleary, Defining random loose packing for nonspherical grains, Phys. Rev. E 83 (2011) 051305.
[8] Y. Yuan, Y. Jiao, Y. Wang, S. Li, Universality of jammed frictional packing, Phys. Rev. Res. 3 (2021) 033084.
[9] D. Robinson, S. Friedman, A. Thomas, D. Hirmas, P. Sullivan, A. Nemes, Soil bulk density and porosity connecting macro-and micro-scales through geometry, Earth Sci. Rev. 268 (2025) 105173.
[10] A.V. Kyrylyuk, A.P. Philipse, Effect of particle shape on the random packing density of amorphous solids, Phys. Status Solidi A 208 (2011) 2299–2302.
[11] L. Onsager, The effects of shape on the interaction of colloidal particles, Ann. N. Y. Acad. Sci. 51 (1949) 627–659.
[12] A.P. Philipse, The random contact equation and its implications for (colloidal) rods in packings, suspensions, and anisotropic powders, Langmuir 12 (1996) 1127–1133.
[13] A. Donev, S. Torquato, F.H. Stillinger, R. Connelly, Jamming in hard sphere and disk packings, J. Appl. Phys. 95 (2004) 989–999.
[14] H. Gould, J. Tobochnik, Thermal and statistical physics 39, Princeton University Press, 2010, pp. 50–52.
[15] M. Jia, W. Xu, Z. Zhu, Numerical study on the excluded volumes of realistic 3D non-convex particles, Powder Technol. 349 (2019) 52–58.
[16] A. Wouterse, S. Luding, A.P. Philipse, On contact numbers in random rod packings, Granul. Matter 11 (2009) 169–177.
[17] A.S. Clarke, H. Jónsson, Structural changes accompanying densification of random hard-sphere packings, Phys. Rev. E 47 (1993) 3975.
[18] A.V. Kyrylyuk, M.A. van de Haar, L. Rossi, A. Wouterse, A.P. Philipse, Isochoric ideality in jammed random packings of non-spherical granular matter, Soft Matter 7 (2011) 1671–1674.
[19] J. Jacquelin, How to Combine Properties of Different Functions into a New Function?, URL (version: 2018-10-24): https://stats.stackexchange.com/q/373387, 2024.
[20] J.R. Koza, Genetic programming as a means for programming computers by natural selection, Stat. Comput. 4 (1994) 87–112.
[21] M. Cranmer, Interpretable Machine Learning for Science with PySR and SymbolicRegression. JL, arXiv preprint arXiv:2305.01582, 2023.
[22] A. Wouterse, Random Packing of Colloids and Granular Matter, Utrecht University, 2008.
[23] F.M. Schaller, S.C. Kapfer, M.E. Evans, M.J. Hoffmann, T. Aste, M. Saadatfar, K. Mecke, G.W. Delaney, G.E. Schröder-Turk, Set Voronoi diagrams of 3D assemblies of aspherical particles, Philos. Mag. 93 (2013) 3993–4017.
[24] S.P. Friedman, D.A. Robinson, Particle shape characterization using angle of repose measurements for predicting the effective permittivity and electrical conductivity of saturated granular media, Water Resour. Res. 38 (2002).
[25] K. Senetakis, M.R. Coop, M.C. Todisco, The inter-particle coefficient of friction at the contacts of Leighton Buzzard sand quartz minerals, Soils Found. 53 (2013) 746–755.
[26] J. Mei, J. Xiao, H. Yang, T. Ye, Q. Meng, Three-dimensional digitalization modeling and simulation of concrete with real recycled aggregates, Comput. Struct. 330 (2026) 108368.
[27] Q. Deng, Y. Zhuang, W. Yang, K. Zhao, S. Zhang, Z. Duan, J. Xiao, Rheological properties of mortar with recycled fine aggregate: from the perspective of particle packing, Constr. Build. Mater. 465 (2025) 140237.
[28] Z. Duan, M. Hou, J. Xiao, Q. Deng, Influences of packing properties on the workability of cementitious materials using mixed recycled fine aggregate derived from decoration waste, Constr. Build. Mater. 458 (2025) 139479.
[29] R.A. Wilkinson, R.P. Behringer, J.T. Jenkins, M.Y. Louge, Granular materials and the risks they pose for success on the moon and mars, in: AIP Conference Proceedings, American Institute of Physics, 2005, pp. 1216–1223.
[30] E. Guyon, J.-Y. Delenne, F. Radjai, Built on Sand: The Science of Granular Materials, Mit Press, 2020.
[31] R. Bagnold, The Physics of Blown Sand and Desert Dunes vol. 265, Methuen & Co, Ltd, London, 1941.
[32] D.J. Jerolmack, K.E. Daniels, Viewing earth's surface as a soft-matter landscape, nature reviews, Physics 1 (2019) 716–730.
[33] G. Tranter, B. Minasny, A. McBratney, B. Murphy, N. McKenzie, M. Grundy, D. Brough, Building and testing conceptual and empirical models for predicting soil bulk density, Soil Use Manag. 23 (2007) 437–443.
[34] D. Robinson, A. Thomas, S. Reinsch, I. Lebron, C. Feeney, L. Maskell, C. Wood, F. Seaton, B. Emmett, B. Cosby, Analytical modelling of soil porosity and bulk density across the soil organic matter and land-use continuum, Sci. Rep. 12 (2022) 1–13.
[35] R.L. Payton, D. Chiarella, A. Kingdon, The influence of grain shape and size on the relationship between porosity and permeability in sandstone: a digital approach, Sci. Rep. 12 (2022) 7531.
[36] G.-y. Li, L.-t. Zhan, Z. Hu, Y.-m. Chen, Effects of particle gradation and geometry on the pore characteristics and water retention curves of granular soils: a combined DEM and PNM investigation: G. Li et al, Granul. Matter 23 (2021) 9.
[37] R. Yang, R. Zou, K. Dong, X. An, A. Yu, Simulation of the packing of cohesive particles, Comput. Phys. Commun. 177 (2007) 206–209.
[38] R. Yang, R. Zou, A. Yu, Effect of material properties on the packing of fine particles, J. Appl. Phys. 94 (2003) 3025–3034.